Click Here for Full Article

Evidence for serpentinite fluid in convergent margin systems: The example of El Salvador (Central America) arc lavas

Sonia Tonarini and Samuele Agostini

Istituto di Geoscienze e Georisorse, Consiglio Nazionale delle Ricerche, Via Moruzzi, 1, I-56124 Pisa, Italy (s.tonarini@igg.cnr.it)

Carlo Doglioni

Dipartimento di Scienze della Terra, Università La Sapienza, Piazzale Aldo Moro, 5, I-00185 Rome, Italy

Fabrizio Innocenti

Dipartimento di Scienze della Terra, Università di Pisa, Via Santa Maria, 53, I-56126 Pisa, Italy

Istituto di Geoscienze e Georisorse, Consiglio Nazionale delle Ricerche, Via Moruzzi, 1, I-56124 Pisa, Italy

Piero Manetti

Istituto di Geoscienze e Georisorse, Consiglio Nazionale delle Ricerche, Via Moruzzi, 1, I-56124 Pisa, Italy

[1] A comprehensive geochemical study, including B, Pb, Sr, and Nd isotopes, has been carried out on El Salvador subduction-related lavas. The rocks have arc-type incompatible element distributions with high LILE/HFSE ratios, nearly constant $^{143}Nd/^{144}Nd$ (≈ 0.5130), and small differences in $^{207}Pb/^{204}Pb$ (15.53–15.57), whereas $^{87}Sr/^{86}Sr$ ranges from 0.7035 to 0.7039. Boron isotopic composition varies widely, between −2.7‰ and +6.3‰. The boron isotope signature points to involvement of fluid inputs from (1) a high-$\delta^{11}B$ serpentinite fluid from serpentized mantle wedge dragged beneath the volcanic arc or from the subducting lithosphere and (2) a low-$\delta^{11}B$ fluid from the progressive dehydration of subducted altered basaltic crust and/or sediments. The observed sample variability is explained with a model in which different proportions of serpentinite-derived (10–50%) and slab-derived fluids are added to an enriched-DMM source, triggering its partial melting. We suggest a model in which tectonic erosion, i.e., dragging down of slivers of serpentinized upper plate mantle, was responsible for the occurrence of serpentinite reservoir, ^{11}B-enriched in the forearc by shallow fluids.

1. Introduction

[2] The geochemical characteristics of arc magmas are commonly interpreted as due to the transfer of subducted material into their source region. An important question concerns the nature and amount of volatiles released during the prograde metamorphic reactions accompanying subduction of the oceanic lithosphere [e.g., *Tatsumi and Eggins*, 1995]. The fluid input to the overlying mantle is considered to be derived from altered oceanic crust (AOC) and its sedimentary cover. However, recent geophysical and geological studies indicate an additional volatile reservoir represented by serpentinized peridotites residing in the subducted lithosphere [e.g., *Rüpke et al.*, 2004; *Ranero et al.*, 2003] and in fore arc mantle [e.g., *Hyndman and Peacock*, 2003; *Hattori and Guillot*, 2003; *Stern et al.*, 2006]. Boron isotope composition is a powerful tool for identifying the nature of subduction components and estimating their relative contributions to arc-magma genesis, because of the large differences in $\delta^{11}B$ between altered oceanic crust and sediments, and the extremely low B content in the pristine mantle, which may be considered as an almost boron-free reservoir [*Leeman and Sisson*, 1996]. The boron isotopic composition of arc magmas is not simply inherited from the subducted materials. Several studies indicate substantial boron loss from slabs in the early stages of subduction by progressive dehydration. This is coupled with boron isotope fractionation: the heavier isotope (^{11}B) partitions preferentially into the fluids [e.g., *Benton et al.*, 2001; *Savov et al.*, 2005]. However, many arc front volcanic rocks exhibit high $\delta^{11}B$ values, which is not to be expected if the slab has been depleted in ^{11}B beneath the forearc. *Peacock and Hervig* [1999] have suggested a model whereby the persisting high $\delta^{11}B$ of arc rocks reflects the presence of hydrated, metasomatized peridotites in the mantle wedge, where B is retained until serpentine breaks down.

[3] The Central America Volcanic Arc (CAVA) is a key area for investigating the role of serpentinized peridotites as fluid sources. In the Central American convergent system, tectonic erosion is an active process [e.g., *Ranero and von Huene*, 2000] and an anomalous wet slab has been postulated to occur [*Abers et al.*, 2003]. Our new data from CAVA can be inserted into an already rich framework of geological, volcanological, geochemical and geophysical data to further understanding of the relative importance of subduction contributions, mantle source characteristics and shallower processes in influencing the genesis of the arc magmas. Numerous papers, including several reviews, have addressed the style of subduction, as well as the along-the-arc variations in dip (and depth) of the subducting slab, the crustal thickness and mantle domains with different geochemical and isotope features. Such studies have progressively introduced new tools and models to detect and better define the processes operating in the CAVA [e.g., *Carr*, 1984; *Feigenson and Carr*, 1986; *Carr and Stoiber*, 1990; *Carr et al.*, 1990, 2004; *Leeman et al.*, 1994; *Reagan et al.*, 1994; *Walker et al.*, 1995, 2000; *Noll et al.*, 1996; *Patino et al.*, 2000; *Chan et al.*, 2002; *Feigenson et al.*, 2004; *Eiler et al.*, 2005].

[4] This paper describes the results of a study of the El Salvador volcanic products representative of a central segment of CAVA. Boron isotope composition data is used in combination with radiogenic isotopes (Sr, Nd and Pb) and trace elements to define the nature and the relative influence of subduction components in the genesis of El Salvador arc lavas.

2. Geodynamic Setting

[5] The Central American subduction system consists of a northeast-directed slab, which is subducted under two continental plates, i.e., Caribbean and North American. The boundary between the two upper plates is located along the Cayman-Motagua sinistral transcurrent fault. The subduction is oblique to the plate boundary (Figure 1) and contains a left-lateral transpressive component. However, inland El Salvador seismicity is characterized by right-lateral focal mechanisms, indicating both transpressional and transtensional tectonics [*DeMets*, 2001; *Dewey et al.*, 2004; *Martínez-Díaz et al.*, 2004; *Corti et al.*, 2005]. The dip of the slab increases from Guatemala ($\sim30°$) to Nicaragua ($\sim60°$) and the related seismicity dies out at the depth of about 200–250 km [*Carr et al.*, 1990; *Protti et al.*, 1995; *Syracuse and Abers*, 2006]. The variation in dip through the northern and central portion the CAVA might be related to the obliquity of the subduction with respect to the absolute motions, as the oblique ramp along a thrust. Age variations along the strike of the oceanic Cocos plate at the trench (23–19 Ma) cannot account for the changing dip of the slab [*Cruciani et al.*, 2005]. The relative motion of Central America over the Cocos plate varies from about 50 mm/yr in the northwest, to 95 mm/yr in the southeast. The convergence rate along the El
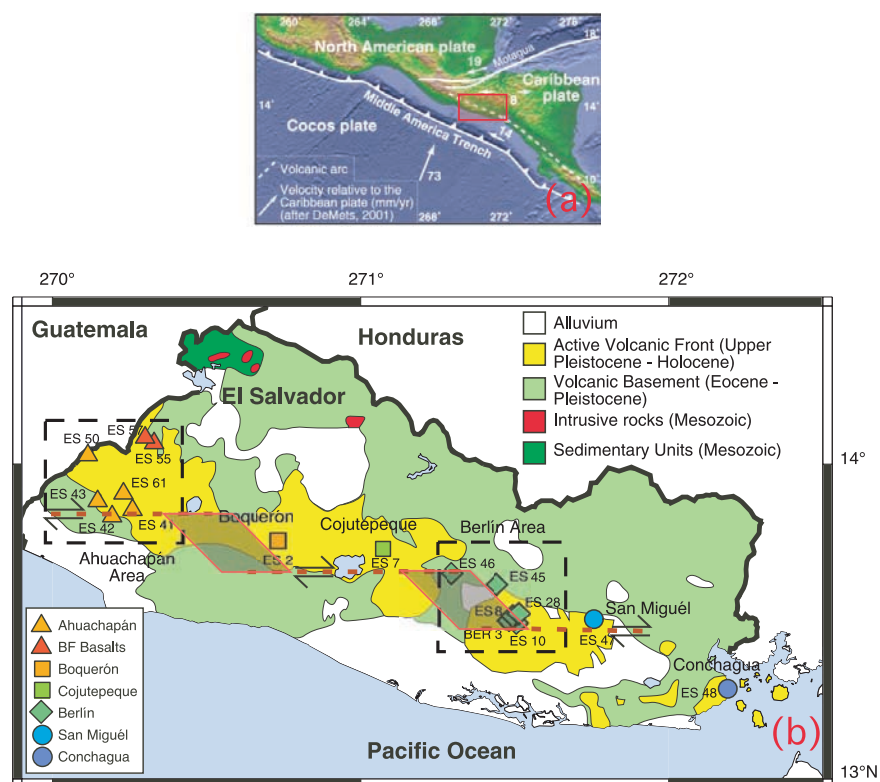
Figure 1. (a) Geodynamic setting of Central America (modified after *Corti et al.* [2005]). Rectangle indicates the area enlarged in Figure 1b. (b) Simplified geological map of El Salvador showing sample distribution. Thick dashed lines represent major segments of El Salvador Fault Zone; grayed areas are major pull-apart basins (taken from *Agostini et al.* [2006]). Dashed boxes enclose the Ahuchapán and Berlín areas. BF basalts are collected behind the volcanic front.

Salvador trench possibly ranges between 75 to 80 mm/yr [*DeMets*, 2001].

[6] The El Salvador volcanic belt is located about 170 km inboard from the trench and about 105 km above the subducting slab [*Syracuse and Abers*, 2006]. Geological and geophysical data have led to the interpretations that the Central America margin is dominated by tectonic erosion and contemporaneous upper plate transtension [e.g., *Aubouin et al.*, 1985; *Ranero and von Huene*, 2000; *Meschede*, 2003; *Vannucchi et al.*, 2004]. Tectonic erosion is a mechanism for removing and transporting to depth forearc mantle lithosphere and even crustal material. The occurrence of forearc material, dragged down by subduction erosion and stored in the supra-slab mantle, has recently been claimed by *Goss and Kay* [2006] to explain the along-arc pattern of Pb-isotopic ratios in southern Central American arc lavas. The shortening of the upper plate, coupled with the low vertical growth of the belt front, supports the existence of tectonic erosion. Indeed, geological and geophysical data have led to interpretations of the evolution of the Central

America margin as a non-accretionary, dominated by tectonic erosion [e.g., *Ranero and von Huene*, 2000; *Meschede*, 2003; *Vannucchi et al.*, 2004].

[7] The subduction zone in the first 50 km from the trench appears then dominated by tectonic erosion, but normal accretion cannot be excluded along some segments, and certainly occurs at deeper depths of the slab. In some places, the decoupling surface is located in the footwall (downgoing plate), resulting in accretion, and in other places, the basal decollement is instead located in the hanging wall (overriding plate), generating tectonic erosion.

[8] In El Salvador, the active deformation takes the form of a major dextral strike-slip fault system, the El Salvador Fault Zone. The fault system is laterally discontinuous, being subdivided into partially overlapping en-echelon segments that form pull-apart structures. Volcanic activity is spatially confined to the fault segments and rarely found in the intervening pull-aparts; no significant temporal gap exists in the erupted products, at least for the Plio-

Quaternary [*Corti et al.*, 2005; *Agostini et al.*, 2006].

[9] *Husen et al.* [2003] proposed a model for central Costa Rica, in which hydrated, serpentinite-and/or chlorite bearing mantle, is in a narrow zone just above the subducting slab and, in a larger area, in the tip of the mantle wedge.

[10] In both the ITRF-NNR (International Terrestrial Reference Frame) (M. Heflin, 2005, http://sideshow.jpl.nasa.gov/mbh/series.html) and the HSRF (Hot Spot Reference Frame) [*Gripp and Gordon*, 2002], North and South America have a different westward velocity component (about 14 mm/yr), in agreement with the extension inferred from seismology in Central America [*DeMets*, 2001] and the lower elevation of CAVA segment of the cordillera. Unlike other models suggesting that oblique subduction causes transtension, we propose that the upper plate transtension is primarily related to the stretching generated by the faster westward advancement of North America relative to South America. This indicates that Central America acts as the transfer zone of the differential motion between the two adjoining larger plates, of North and South America. Central America therefore appears to be an area where two independent geodynamic settings coexist, the oblique subduction and the transtension in the overriding plate, the latter being related to the different far field velocities of the adjoining plates.

3. Sampling and Sample Descriptions

[11] The samples selected for this study are a subset of 54 rocks from the entire El Salvador active segment, whose petrography and chemistry are reported by *Agostini et al.* [2006]. Two volcanically active areas, Berlín in the east and Ahuachapán in the west, were investigated in detail, including the local volcanic basement, known as the Miocene to Pleistocene Balsamo Formation (Figure 1). In the Berlín area active deformation is controlled by the regional stress field, resulting in the development of transcurrent systems of right-lateral EW-trending strike-slip faults. On the other hand, the structural setting of the Ahuachapán area is more complex, reflecting interaction among different stress fields.

[12] In the Ahuachapán area, several strato-volcanoes formed over a local volcanic basement (i.e., ES 43: 248 ± 67 ka [*Agostini et al.*, 2006]) and were dissected by a major caldera event related to the emission of abundant pyroclastic products [*Gonzales Partida et al.*, 1997]. An ^{40}Ar-^{39}Ar age of 127 ± 20 ka was obtained for a pre-caldera lava. The youngest products are represented by small cones, domes and minor lava flows. In this area, two samples from the basement (ES 43 and ES 50), and three representative of younger activity (ES 41, ES 42 and ES 61) were selected for geochemical analyses. Another two samples (ES 55 and ES 57) from monogenetic cones with associated lava flows were taken as representative of the infrequent volcanic activity about 15 km beyond the volcanic front (hereafter BF basalts; Figure 1b).

[13] In the Berlín area, a caldera structure has affected an old Pleistocene strato-volcano. The caldera-forming eruption produced large quantities of pyroclastic deposits with an age of about 100 ka [*D'Amore and Mejia*, 1999]. The Balsamo volcanic basement sampled close to Río Lempa dates back to 415 ± 27 ka (sample ES 46). Two lavas (ES 8 and ES 28) and a glass-rich fragment from a pyroclastic flow (ES 10) were chosen as representative of the post-caldera products. Samples BER 3, ES 7, ES 45 and ES 46 are representative of the basement. Other samples from the active volcanic front (ES 2, from Boquerón, ES 47 from San Miguél and ES 48 from Conchagua) were chosen in order to obtain a more comprehensive sampling along the arc. The composition of the selected samples covers a wide range, from basalts to dacites (Figure 2). In the Berlín area, basaltic products occur only in the Balsamo formation, while they are lacking in the younger products. The alkali content of the basalts varies widely. In particular, the two samples from the BF monogenetic cones (ES 55 and ES 57) show a higher alkali/SiO_2 ratio, whereas the samples from the easternmost part of El Salvador (ES 47 and ES 48) have the lowest alkali contents. Basalts and basaltic andesites have a porphyritic texture, with a phenocryst assemblage characterized by abundant augitic clinopyroxene, plagioclase and olivine, except for BF samples, in which Mg-rich olivine is the only phenocryst. Plagioclase is the dominant phase in more evolved rocks, along with ortho- and clinopyroxene. Quartz and sanidine can occur in dacites, and sporadic amphibole is also present. Petrographical observation reveals that the groundmasses usually contain different amounts of well-preserved glass, which becomes more abundant in the most evolved rocks. Intensive parameters were assessed using different geo-thermobarometers [*Agostini et al.*, 2006]. Overall, the observed paragenesis developed under shallow conditions ($P \leq 0.5$ GPa), with $fO_2 \approx +1/+2$
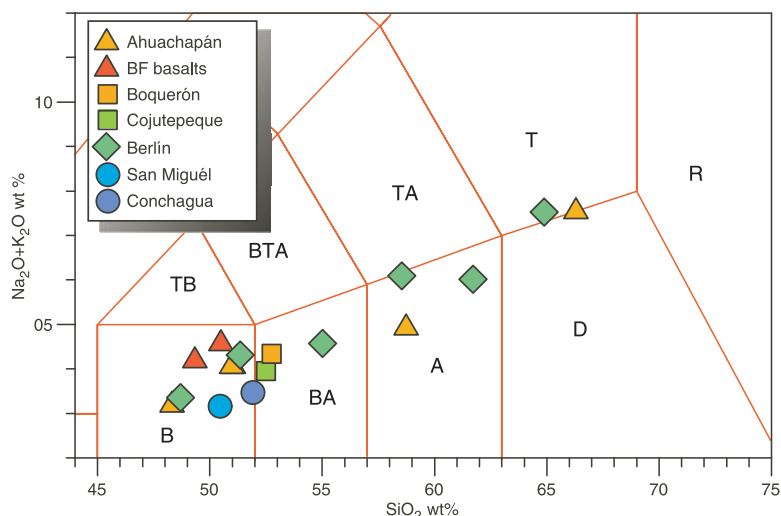
Figure 2. Total alkali versus silica classification diagram for El Salvador volcanic rocks (fields after *Le Maitre* [2002]).

Δ_{FMQ} in the basalt-dacite range, and H_2O content around 3–4% in andesite and dacites.

4. Analytical Methods

[14] Trace elements (except B) were determined via ICP-MS (Fisons PQ2 Plus®) at the University of Pisa, Department of Earth Sciences. Analytical precisions, evaluated by repeated analyses of the in-house standard HE-1 (Mt. Etna hawaiite) generally resulted between 2 and 5% RSD, except for Gd (6%), Tm (7%), Pb and Sc (8%). Detection limits at the 6σ level are in the range of 2–20 ppb for all elements, except Ba, Pb and Sr (100–200 ppb) [*D'Orazio*, 1995].

[15] Sr and Nd isotope ratios were determined via TIMS techniques at the Pisa Istituto di Geoscienze e Georisorse of C.N.R. (Italian National Research Council) using a Finnigan MAT 262 multicollector mass spectrometer running in dynamic mode. The measured $^{87}Sr/^{86}Sr$ ratios have been normalized to $^{86}Sr/^{88}Sr = 0.1194$ and $^{143}Nd/^{144}Nd$ ratios to $^{146}Nd/^{144}Nd = 0.7219$. During the measurement period, the mean measured value of $^{87}Sr/^{86}Sr$ for the NIST–SRM 987 standard was 0.710242 ± 0.000013 (2SD, N = 25), while the mean $^{143}Nd/^{144}Nd$ for the La Jolla standard was 0.511847 ± 0.000008 (2SD, N = 25). The JNdi-1 standard [*Tanaka et al.*, 2000] was also analyzed and yielded a $^{143}Nd/^{144}Nd$ value of 0.512100 ± 0.000010 (2SD, N = 25). The total procedure blanks, ≈ 0.5 ng and 0.1 ng of Sr and Nd, respectively, were negligible for the analyzed samples. Lead was extracted by chromatographic ion ex-

change in Dowex 1 anion resin, using standard HBr and HCl elution procedures. Isotopic analyses were performed via TIMS techniques with a Finnigan MAT 262 multicollector mass spectrometer, operating in static mode. Replicate analyses of Pb standard NIST–SRM 981 indicated that Pb isotope ratios are accurate to within 0.025% (2SD) per mass unit, after applying mass discrimination corrections of $0.14 \pm 0.01\%$ per mass unit relative to the reference composition from *Todt et al.* [1993]. The Pb blank varies from about 0.4 to 0.6 ng, and no blank correction was made. Boron isotope composition was determined using a VG 54E mass spectrometer after boron extraction by alkaline fusion followed by ion-exchange purification. The data is reported in the conventional delta notation ($\delta^{11}B$) as per mil (‰) deviation from the accepted composition of NIST–SRM 951 (certified $^{11}B/^{10}B = 4.04362$ [*Catanzaro et al.*, 1970]). The reproducibility of isotopically homogeneous samples treated with alkaline fusion chemistry is approximately ±0.5‰ (2SD), and replicate analyses of samples agree within this limit. Further analytical details are given by *Tonarini et al.* [2003]. Boron concentration was determined by isotope dilution; the analytical uncertainty is estimated to be ±5% on the basis of replicate analyses (this conservative error has been ascribed almost entirely to the alkaline fusion of the sample before adding the spike solution).

5. Results

[16] Major and trace elements and isotope data for studied samples are reported in Table 1. Compatible

Table 1. Major and Trace Elements and Sr, Nd, Pb, and B Isotope Data

Label	ES 50	ES 43	ES 42	ES 41	ES 61	ES 55	ES 57	ES 7	ES 2	ES 45	BER 3	ES 46	ES 28	ES 8	ES 10	ES 47	ES 48
SiO_2, wt%	57.42	50.03	47.72	49.62	65.09	49.64	48.41	51.35	52.3	47.63	51.19	60.82	54.15	57.97	63.90	49.74	51.19
TiO_2	0.59	0.91	1.08	0.92	0.51	1.25	1.31	0.85	1.12	1.07	1.14	0.70	0.76	0.90	0.66	0.95	0.83
Al_2O_3	18.04	18.53	17.29	18.28	15.72	17.30	16.64	17.78	18.33	18.58	17.55	17.46	17.77	17.28	16.57	19.68	19.09
Fe_2O_3	3.20	3.25	4.35	3.18	1.93	1.27	6.38	9.93	2.31	5.84	11.70	3.81	3.60	8.06	1.19	4.05	3.53
FeO	3.40	6.70	7.74	6.76	2.67	7.56	3.05		7.90	6.05		2.72	5.32		3.50	6.10	6.49
MnO	0.14	0.18	0.19	0.18	0.11	0.15	0.15	0.15	0.19	0.19	0.20	0.13	0.17	0.22	0.19	0.16	0.18
MgO	3.01	4.56	6.91	4.61	1.26	7.32	8.27	4.26	3.68	4.31	3.99	1.61	3.91	2.43	1.32	4.14	4.58
CaO	6.91	9.59	10.10	9.57	3.30	8.95	9.42	9.47	8.81	10.60	9.24	5.15	8.00	5.75	3.48	10.50	9.15
Na_2O	3.45	2.84	2.62	2.84	4.71	3.36	3.09	2.50	3.18	2.63	2.78	4.24	2.96	4.49	5.11	2.46	2.70
K_2O	1.43	1.20	0.60	1.17	2.76	1.20	1.08	1.42	1.18	0.67	1.54	1.71	1.56	1.56	2.32	0.72	0.78
P_2O_5	0.18	0.21	0.15	0.21	0.12	0.33	0.32	0.19	0.23	0.24	0.34	0.20	0.19	0.34	0.22	0.18	0.18
L.O.I.	1.31	1.01	0.65	0.75	0.55	0.59	0.65	0.70	0.53	0.82	0.07	1.03	0.45	0.29	0.75	0.48	0.64
Total	99.08	99.01	99.4	98.09	98.73	98.92	98.77	98.6	99.76	98.63	99.74	99.58	98.84	99.29	99.21	99.16	99.34
Be, ppm	0.76	0.82	0.48	0.78	1.44	1.19	1.23	0.71	0.76	0.55	1.38	1.11	0.82	0.98	1.32	0.51	0.61
Sc	15.7	30.9	44.6	28.5	13.2	25.8	28.3	29.8	28.1	34.7	22.0	16.2	24.6	24.0	17.2	32.5	25.5
V	141	253	343	292	74	217	216	236	262	320	132	103	209	106	35	334	282
Cr	8.22	51.0	25.8	13.4	2.75	243	324	10.0	4.01	7.92	2.62	1.09	3.74	1.81	0.67	16.2	13.6
Co	19.3	30.7	46.4	32.3	9.5	35.7	39.5	30.1	26.0	31.8	15.9	10.3	27.1	42.1	4.8	27.2	30.0
Ni	11	30	23	14	4	116	139	17	7	10	4	3	11	3	2	10	12
Cu	57	121	109	105	46	53	63	82	103	156	40	7	221	18	9	182	95
Ga	18.3	17.9	18.0	18.2	16.9	16.6	16.1	17.5	18.5	18.2	19.0	16.8	16.8	18.0	17.2	19.0	17.7
Rb	20.6	27.3	6.0	26.4	65.4	18.2	20.1	30.3	22.2	12.6	50.4	29.4	30.2	28.5	44.3	11.5	10.8
Sr	490	592	393	594	232	571	543	468	479	688	482	483	467	513	363	509	518
Y	18.5	23.4	21.6	23.0	34.0	25.0	24.5	22.5	31.0	19.6	38.5	25.1	23.5	33.9	37.4	20.7	22.1
Zr	96	75	56	73	212	141	132	104	103	48	169	115	109	108	154	53	54
Nb	2.05	1.50	1.30	1.48	4.24	7.98	8.60	2.23	2.03	1.21	4.11	2.65	2.53	2.48	3.38	1.29	1.45
Cs	1.25	1.18	0.17	1.19	1.31	0.30	0.38	0.55	1.15	0.49	2.69	0.53	0.73	1.54	2.35	0.62	0.30
Ba	589	477	309	484	1019	364	272	580	528	397	1032	893	712	870	1135	422	501
La	7.9	10.4	5.6	10.4	16.1	14.1	13.0	10.0	9.0	7.5	18.3	13.3	10.4	12.2	14.4	6.2	7.6
Ce	17.9	23.0	12.4	23.5	33.5	31.6	29.2	21.8	21.9	17.1	41.3	23.8	23.2	27.5	32.8	14.6	15.0
Pr	2.57	3.49	2.03	3.42	4.57	4.35	4.07	3.27	3.38	2.70	6.15	4.18	3.44	4.43	4.97	2.32	2.56
Nd	11.6	15.6	9.8	15.9	19.7	19.3	18.1	14.6	16.6	13.1	28.0	18.8	15.4	20.8	22.4	11.3	12.3
Sm	2.92	3.92	2.89	3.88	4.68	4.59	4.27	3.74	4.58	3.44	6.83	4.56	3.74	5.51	5.73	3.21	3.28
Eu	0.91	1.29	1.08	1.25	1.02	1.46	1.45	0.94	1.27	1.28	1.66	1.28	0.91	1.57	1.38	1.07	1.07
Gd	3.03	4.05	3.38	4.07	4.80	4.62	4.49	3.88	5.09	3.67	6.87	4.47	3.95	5.99	6.07	3.49	3.54
Tb	0.50	0.66	0.57	0.66	0.85	0.75	0.74	0.62	0.85	0.58	1.08	0.71	0.64	0.95	1.00	0.60	0.61
Dy	3.04	3.89	3.53	3.96	5.17	4.34	4.23	3.73	5.25	3.39	6.52	4.17	3.78	5.62	6.04	3.60	3.64
Ho	0.65	0.83	0.76	0.84	1.14	0.88	0.87	0.78	1.13	0.71	1.37	0.86	0.80	1.20	1.31	0.74	0.76
Er	1.81	2.19	2.12	2.23	3.31	2.42	2.35	2.16	3.11	1.85	3.78	2.39	2.27	3.28	3.68	2.05	2.08

Table 1. (continued)

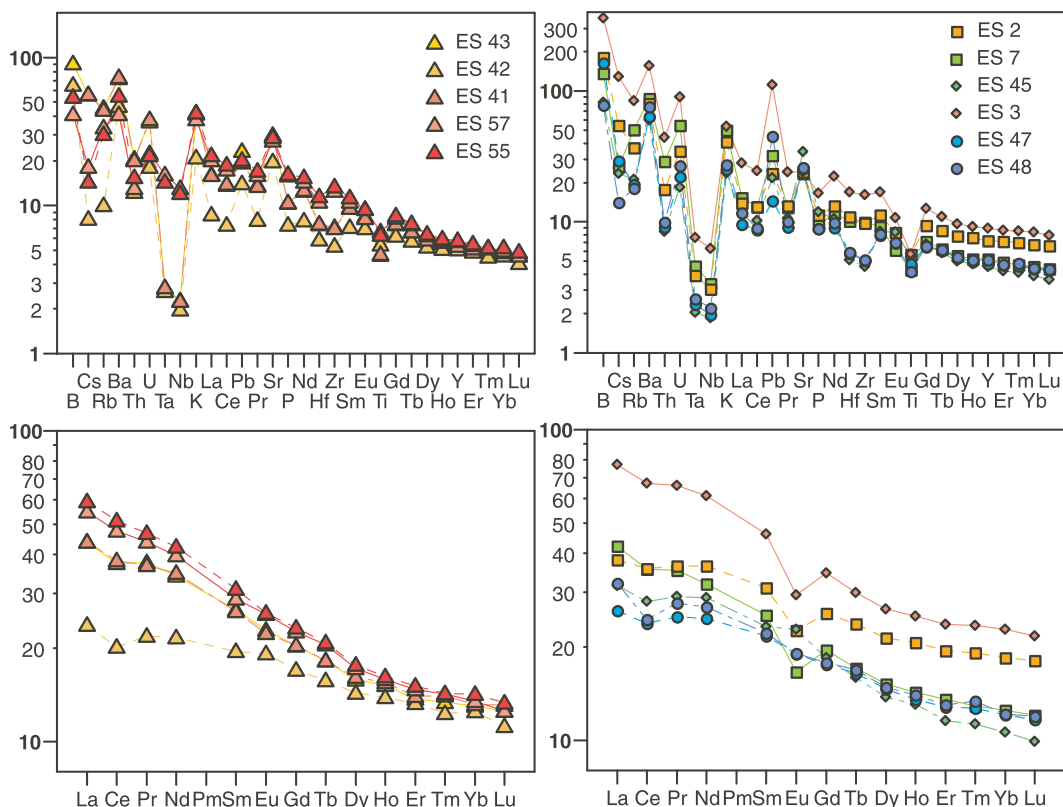| Label	ES 50	ES 43	ES 42	ES 41	ES 61	ES 55	ES 57	ES 7	ES 2	ES 45	BER 3	ES 46	ES 28	ES 8	ES 10	ES 47	ES 48
Tm	0.28	0.33	0.31	0.35	0.54	0.35	0.35	0.32	0.47	0.28	0.58	0.38	0.35	0.48	0.56	0.31	0.33
Yb	1.77	2.10	2.01	2.12	3.48	2.29	2.17	2.01	2.97	1.71	3.67	2.46	2.28	3.03	3.63	1.94	1.96
Lu	0.26	0.31	0.27	0.32	0.53	0.33	0.31	0.30	0.44	0.24	0.53	0.38	0.34	0.46	0.56	0.29	0.29
Hf	2.74	2.11	1.66	2.13	5.72	3.24	2.97	2.88	3.09	1.44	4.80	3.08	3.04	3.32	4.54	1.63	1.65
Ta	0.15	0.10	0.10	0.10	0.34	0.53	0.59	0.17	0.14	0.07	0.28	0.20	0.17	0.18	0.23	0.09	0.10
Tl	0.17	0.12	0.03	0.14	0.27	0.15	0.07	0.10	0.11	0.03	0.12	0.09	0.16	0.08	0.26	0.03	0.07
Pb	4.2	3.5	2.1	2.9	6.3	3.0	2.9	4.8	3.5	3.3	16.7	4.9	31.4	4.6	7.8	2.2	6.8
Th	1.18	1.64	0.98	1.60	4.32	1.23	1.04	2.29	1.41	0.67	3.53	1.95	2.06	1.98	2.91	0.73	0.79
U	0.52	0.75	0.37	0.77	2.04	0.44	0.45	1.12	0.70	0.37	1.84	0.98	1.08	1.04	1.56	0.45	0.54
B	22.60	9.10	6.53		21.60	5.39	4.83	13.69	18.00	8.16	36.10	9.98	20.20	18.20	33.20	16.40	7.80
$^{87}Sr/^{86}Sr$	0.703582	0.703660	0.703666	0.703655	0.703574	0.703585	0.703524	0.703850	0.703777	0.703805	0.703874	0.703816	0.703898	0.703863	0.703867	0.703868	0.703851
$^{143}Nd/^{144}Nd$	0.512997	0.512993	0.513013	0.513002	0.512997	0.512947	0.512954	0.512999	0.512995	0.512999	0.513012	0.512975	0.513002	0.513006	0.512997	0.512993	0.513014
$^{208}Pb/^{204}Pb$	38.324	38.257	38.300	38.287	38.357	38.320	38.277	38.239	38.239	37.907 / 37.887	38.231	38.273	38.262	38.184	38.190	38.197	38.187
$^{207}Pb/^{204}Pb$	15.566	15.554	15.557	15.566	15.570	15.574	15.559	15.552	15.550	15.540 / 15.534	15.548	15.557	15.540	15.540	15.538	15.543	15.544
$^{206}Pb/^{204}Pb$	18.651	18.588	18.637	18.600	18.676	18.619	18.618	18.570	18.574	18.193 / 18.190	18.565	18.596	18.587	18.531	18.547	18.538	18.528
$\delta^{11}B‰$	3.1	4.1	2.3 / 1.8		2.8	−0.4 / −0.8	−2.7 / −2.8	5.8	4.2	0.8 / 0.3 / 0.5	6.3	5.3	6.1	6.3	5.9	5.2	2.1 / 2.8

Figure 3. Primitive mantle (PM)–normalized trace element variation diagrams and chondrite-normalized rare earth element (REE) diagrams for El Salvador volcanics. Normalization values after *McDonough and Sun* [1995]. Scale for abundances on the *y axis* is logarithmic.

elements such as Sc, V, Co, Ni and Cr show a negative correlation to SiO_2. Ni and Cr in basaltic rocks are under 30 and 51 ppm, respectively, except for the two BF samples ES 55 and ES 57, which yielded Cr > 240 and Ni > 115 ppm.

[17] The samples exhibit arc-type incompatible element distribution with LILE (Large Ion Lithophile Elements) to HFSE (High Field Strength Elements) ratios higher than the primitive mantle values. The incompatible elements generally increase with increasing SiO_2, though a large dispersion is observed in less evolved rocks. In the primitive mantle–normalized plot (Figure 3), basalts are characterized by variable enrichments in LILE as well as B over HFSE (e.g., Nb, Ta, Zr, Ti). The trace element patterns show positive spikes decreasing from B, Ba, Pb, U, K to Sr, and negative Nb, Ta, Ti, Hf and Zr anomalies (Figure 3); BF basalts (ES 55 and ES 57) show higher abundances of Nb, Ta, and to a lesser extent, other HFSE. Chondrite-normalized rare earth element (REE) patterns (Figure 3) are LREE enriched $((La/Yb)_N = 1.9–4.2)$. Three samples exhibit pronounced Eu negative anomalies, $(Eu_N/Eu^*) < 0.8$,

reflecting plagioclase fractionation. BF basalts yielded the highest LREE/HREE and MREE/HREE ratios, with $(La/Yb)_N \approx 4.2$ and $(Sm/Yb)_N \approx 2.1$. Other basalts show less REE fractionation, with $(La/Yb)_N < 3.4$ and $(La/Sm)_N < (Sm/Yb)_N$; this is particularly evident in the pattern of sample ES 45 from the Balsamo formation in the Berlín area. Moreover, some basalts show a slight negative Ce anomaly. The occurrence of a Ce anomaly in samples where evidence of REE redistribution is lacking [*Patino et al.*, 2003] may be linked to the decoupling of Ce from other REEs during weathering, resulting from the oxidation of Ce^{3+} to Ce^{4+} and subsequent cerium precipitation under high-fO_2 conditions [*Dia et al.*, 2000].

[18] The Sr and Nd isotopes are plotted in Figure 4. Sr variations are relatively large ($^{87}Sr/^{86}Sr$ from 0.70352 to 0.70390), while the Nd isotope ratio is nearly constant ($^{143}Nd/^{144}Nd$ around 0.51300), except for the two monogenetic BF basalts, which have slightly lower $^{143}Nd/^{144}Nd$ (Figure 4). As stressed by *Agostini et al.* [2006], the lack of any correlation between the degree of evolution and $^{87}Sr/^{86}Sr$ ratios indicates that crustal contamination
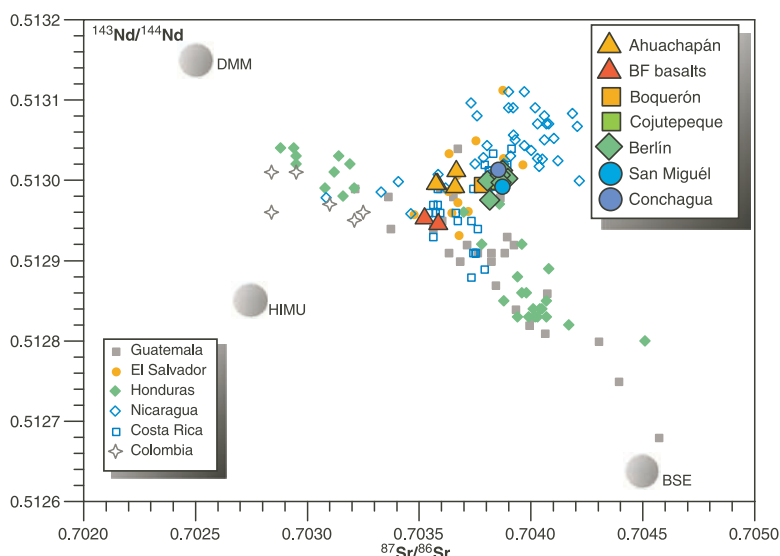
Figure 4. Strontium-neodymium isotope diagram for Central American volcanic rocks. El Salvador samples from this study are indicated by larger symbols. Samples labeled Colombia are from La Providencia island (Caribbean Sea, offshore of Nicaragua). Literature data for Central America volcanics have been taken from M. J. Carr's database available at http://www.rci.rutgers.edu/~carr/index.html. DMM, depleted MORB mantle; BSE, bulk silicate Earth; HIMU, high U/Pb ratio (μ) mantle components.

processes are likely to be minimal. With the exception of one basalt from the Berlín basement (ES 45), the lead isotope ratios fall within a narrow range (Table 1). Despite their limited variation, significant negative correlation is observed between $^{206}Pb/^{204}Pb$ and $^{87}Sr/^{86}Sr$ ratios with samples from western El Salvador having higher Pb but lower Sr isotopic ratios than samples from eastern El Salvador (Figure 5).

[19] The boron content ranges between 4.8 to 36.1 ppm and yields a weak positive correlation with the degree of fractionation. Boron isotope composition varies widely, ranging from −2.7‰ to +6.3‰. Figure 6 shows the variation in $\delta^{11}B$ versus SiO_2 content and demonstrates that the less evolved rocks exhibit the entire range of isotope variability. In the Berlín volcanic system, the most evolved rocks, produced by crystal fractionation processes, display the same $\delta^{11}B$ as the Berlín basalts. The
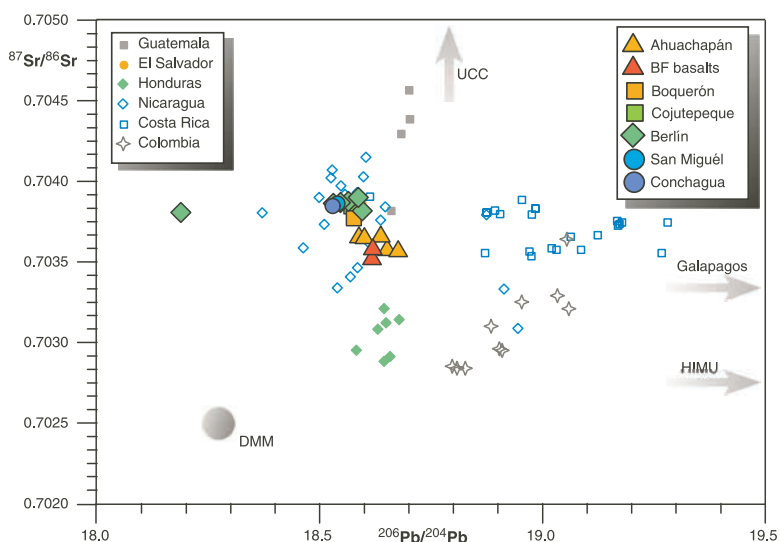

Figure 5. Plot of $^{87}Sr/^{86}Sr$ versus $^{206}Pb/^{204}Pb$ for Central American lavas. UCC, upper continental crust [*Taylor and McLennan*, 1995].
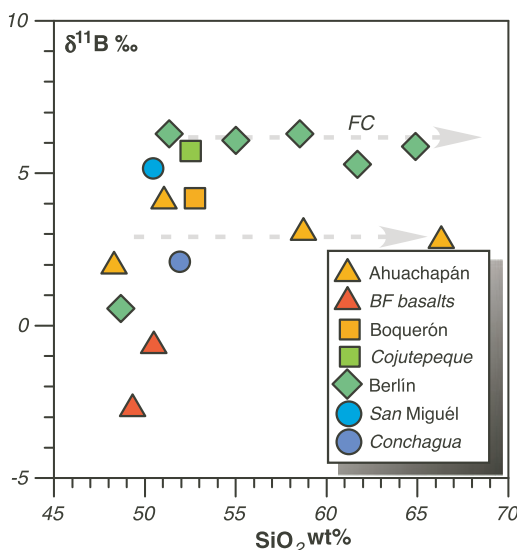
Figure 6. Plot of $\delta^{11}B$ against SiO_2 for analyzed samples of El Salvador volcanics. *FC*, fractional crystallization trend.

Ahuachapán andesite and dacite yield $\delta^{11}B$ values (+2.8‰ to +3.1‰) within the same range as basalts from the same area (2.0‰ and 4.1‰), but the two BF samples, ES 55 and ES 57, are characterized by negative $\delta^{11}B$ (−0.6‰ and −2.7‰, respectively).

6. Discussion

[20] The Central American arc lavas display systematic geochemical variations along the volcanic front, most of which are considered to reflect variations in the subduction component (i.e., Ba/La, U/Th, $^{10}Be/^9Be$, and $^{87}Sr/^{86}Sr$ ratios) [*Carr et al.*, 2004]. Several distinct components added in different proportions to several types of mantle wedge have been invoked to explain the observed regional trends. Such components include fluids released by subducted altered oceanic crust (AOC) and/or by serpentinized lithosphere [*Rüpke et al.*, 2002], as well as fluids derived from, or bulk mixing with, sediments whose composition has been inferred from drilling data (DSDP 495) obtained offshore of Guatemala [*Morris et al.*, 1990; *Patino et al.*, 2000]. Moreover, the relatively high $^{206}Pb/^{204}Pb$ values found in Costa Rica lavas were interpreted by *Feigenson et al.* [2004] as due to the presence of a Galapagos-influenced mantle component (Figure 5). The small Sr and Pb isotopic variations have been attributed to crustal contamination in some Guatemala and Honduras lavas [*Carr et al.*, 2004].

[21] Our detailed geochemical investigation of the El Salvador segment of the CAVA allows us to trace the transfer of slab-derived elements into the mantle wedge beneath El Salvador.

6.1. Subduction Component Sources

[22] In several Pacific arcs, a positive correlation between $\delta^{11}B$ and B/Nb has been described and interpreted as reflecting mixing relations between a mantle source and a fluid with near constant $\delta^{11}B$, considered representative of the subduction component [*Palmer*, 1991; *Ishikawa and Nakamura*, 1994; *Ishikawa and Tera*, 1997, 1999; *Ishikawa et al.*, 2001]. In El Salvador, a relatively poor positive correlation is observed between $\delta^{11}B$ and the ratios of fluid mobile elements to fluid immobile elements, such as B/Nb (Figure 7), Rb/Nb and Ba/Zr (not shown). Thus the data is not consistent with the hypothesis of simple mixing between a B-poor mantle and a homogeneous B-rich fluid. Instead, the measured $\delta^{11}B$ can be explained by assuming a metasomatizing agent with an isotopic composition ranging from ≈+7‰ (Berlín samples, including Cojutepeque and San Miguel volcanoes) and ≈+2‰ (Ahuachapán and Conchagua samples). Sample ES 45 from Berlín volcanic basement is characterized by an $\delta^{11}B$ of +0.6‰, suggesting that fluid with lower $\delta^{11}B$ could have affected the mantle-source region before the inception of present activity.

[23] Similar isotope variations with $\delta^{11}B$ values as high as +6/ +7‰ have been found in some Pacific

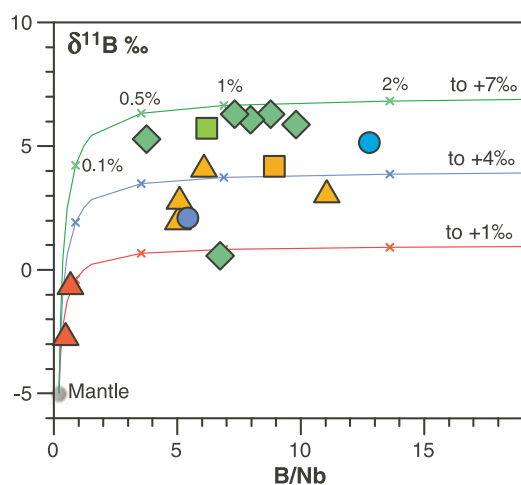**Figure 7.** Diagram of $\delta^{11}B$ versus B/Nb for El Salvador lavas (symbols as in Figure 6). Mixing lines between mantle ($\delta^{11}B = -5$ and B/Nb = 0.2) and fluids with a B/Nb ratio of 1000 and $\delta^{11}B$ of +1, +4, and +7‰ are shown.

arcs (Tonga, Mariana, Kamchatka, Kurile [*Ishikawa and Nakamura*, 1994; *Ishikawa and Tera*, 1997, 1999; *Ishikawa et al.*, 2001]). Such high ratios have been attributed to fluid derived from dehydration of altered oceanic crust enriched in B from seawater ($\delta^{11}B$ of AOC between +17 and +4‰ with an average value of 5.3‰ [*Spivack and Edmond*, 1987; *Smith et al.*, 1995]). However, it is unlikely that high $\delta^{11}B$ persists at P-T conditions in the slab under the volcanic front, because most of the B (^{11}B-enriched) is released at low T in the early stages of subduction and stored mainly in clay minerals and pore waters [see, e.g., *Moran et al.*, 1992; *Leeman and Sisson*, 1996]. Boron loss is coupled with isotopic fractionation, since ^{11}B is preferentially partitioned in the fluid phase [*Benton et al.*, 2001] and leaves the residual slab progressively more ^{11}B-depleted [*Rose et al.*, 2001; *Bebout and Nakamura*, 2003; *Tonarini et al.*, 2005].

[24] Subducted sediments also appear to be an unlikely source of ^{11}B. Boron is present in two forms in marine sediments. The first component is desorbable boron ($\delta^{11}B \approx +15$‰ [*Spivack and Edmond*, 1987]), which is largely lost at shallow depths, as demonstrated by the experiments of *You et al.* [1995]. The second component is structurally bound boron, which is isotopically heterogeneous and affected by isotopic fractionation during metamorphism accompanying subduction, as occurs for AOC. Thus metamorphosed sediments should have much lower B (and ^{11}B) than unmetamorphosed ones. Models involving mixing between mantle and metamorphosed bulk sediments (such as the DSDP 495 sediment column [*Patino et al.*, 2000]) failed to produce the high source B-enrichment needed to generate most of the El Salvador lavas, whereas addition of 2–3% fluid to mantle reservoir is sufficient to match the B/La ratios observed in the lavas [*Leeman et al.*, 1994].

[25] An alternative ^{11}B-rich reservoir is represented by serpentinized peridotites of the oceanic lithosphere (B = 30–140 ppm [*Bonatti et al.*, 1984; W. P. Leeman, personal communication, 2005]; $\delta^{11}B \approx +10$‰ [*Tonarini et al.*, 2006]), where B is hosted by serpentine, which is stable down to 3–4 GPa at $\approx 650°C$ [*Ulmer and Trommsdorff*, 1995]. Serpentine may reside in the subducted oceanic lithosphere [e.g., *Ranero et al.*, 2003] or be generated in the forearc by dehydration fluids and dragged down by subduction-induced mantle flow [e.g., *Hattori and Guillot*, 2003]. Such a reservoir was sampled in the Mariana forearc, where it is char-

acterized by average B and $\delta^{11}B$ values of 27 ppm and +14‰, respectively [*Benton et al.*, 2001].

6.2. Fluid Origins and Role in Magma Genesis

[26] The fluids metasomatizing the CAVA mantle wedge may be a composite of fluids derived from the dehydration of subducted crust and serpentinized ultramafic rocks. Indeed, a roughly linear correlation between Sr and B isotopes can be observed (Figure 8). However, this correlation cannot be explained by simple binary mixing between a mantle end-member (with low $\delta^{11}B$ and $^{87}Sr/^{86}Sr$) and a fluid (with high $\delta^{11}B$ and $^{87}Sr/^{86}Sr$), because the large differences in their B/Sr ratios would not produce a line, but instead a strongly convex hyperbolic curve. Moreover, a two components mixing is unable to explain the B/Nb and $\delta^{11}B$ variations. In order to define the geochemical features of the subduction-related components and their relative contributions to magma genesis, we modeled the Sr and B isotopic composition of fluids from the different reservoirs and their subsequent addition to the mantle source, beneath the volcanic front. The composition of the end-members and the model results are reported in Table 2 and plotted in Figure 8. El Salvador-Guatemala mantle wedge has been considered a subduction modified depleted mantle [e.g., *Carr et al.*, 2004; *Eiler et al.*, 2005], whereas other authors [e.g., *Patino et al.*, 2000] have proposed an E-MORB–like mantle as the primary source of CAVA magmas. Because of almost constant Nd isotope ratios of VF lavas (≈ 0.51300), in the model we choose the E-DMM [*Workman and Hart*, 2005] as representative of mantle source prior to the subduction. In any case, the mantle (both depleted and enriched) is characterized by very low boron content, thus only a slightly smaller amount of fluid needs to be added to magma source, if a higher $^{87}Sr/^{86}Sr$ mantle ratio is assumed for the mantle wedge source.

[27] The Sr and B isotope compositions of the fluids were calculated assuming a subducted crust composed of 80% altered basalts and 20% sediments. The AOC+Sed derived fluid was mixed in different proportions with a serpentinite-derived fluid. The observed $\delta^{11}B$ and $^{87}Sr/^{86}Sr$ co-variation in El Salvador lavas is explained as the result of the addition to the mantle of about 1–3% of fluids with a serpentinite component varying from 10% to 50%. In the volcanic front samples, B isotope
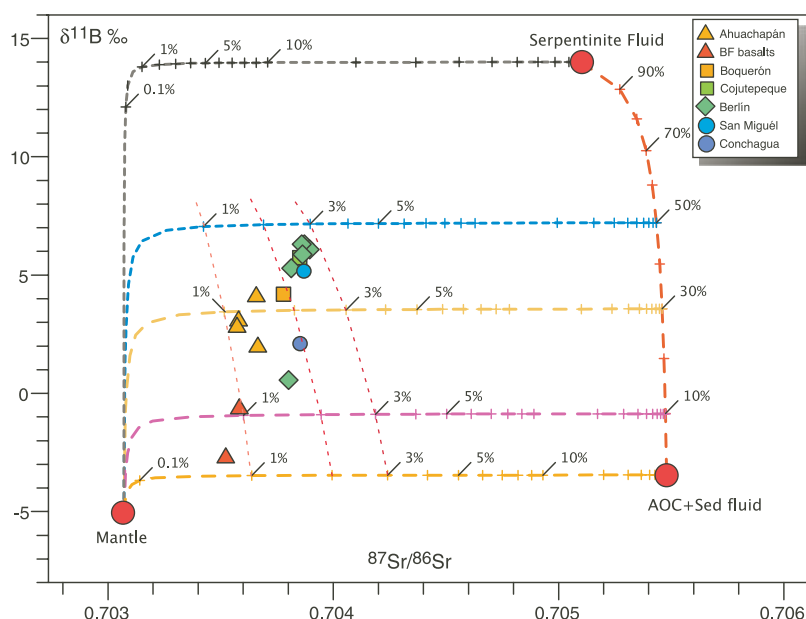
Figure 8. Model of mantle source metasomatism by serpentinite and AOC + Sediment fluids using the δ^{11}B versus ^{87}Sr/^{86}Sr diagram. Data sources for mantle, serpentinite fluid, and slab fluid are in Table 2. Mixing lines between mantle source (E-DMM, from *Workman and Hart* [2005]) and variable proportions of slab-serpentinite fluids are plotted (for 10%, 30%, and 50% of serpentinite fluid); simple binary mixing lines between the three end-members are also shown. Thinner dashed lines connect equivalent amounts of total fluid added to the mantle source. Composition of AOC+Sediment fluid is calculated at 650°C and 120 km after six subsequent stages of dehydration (see Table 2). Numbers on the mixing trajectories represent amount of fluid.

variability is positively correlated with the amount of fluids from serpentine breakdown. Although these values are model-dependent, and especially sensitive to the assumed fluid compositions, they do provide an indication of relative degree of source modification.

[28] Hence, on the basis of B-Sr isotopic signatures, the El Salvador lavas seem to be derived

Table 2. Model Parameters Used for Mixing Calculations

	Mantle[a]	DSDP 495 Sediment[b]	AOC[c]	Forearc Serpentinites[d]	D$_{(sol/fluid)}$	AOC + Sed a[e]	AOC + Sed b[e]	AOC + Sed c[e]	Serp. Fluid
B	0.03	75	26	27	0.1	240	201	172	270
Sr	9.7	336	120	20	0.5	310	303	298	40
Nd	0.7	19	6.5	0.008	1	9.5	9.7	9.9	0.004
Pb	0.024	9.6	0.2	0.04	0.5	3.94	3.86	3.80	0.08
δ^{11}B	−5	−1	5.5	14		22.5	7.7	−3.5	14
^{87}Sr/^{86}Sr	0.70307	0.7076	0.704	0.7051		0.70548	0.70548	0.70548	0.7051
^{143}Nd/^{144}Nd	0.513	0.51274	0.51305	0.5131		0.512919	0.512919	0.512919	
^{207}Pb/^{204}Pb	15.568	15.63	15.5			15.62	15.62	15.62	

[a] Mantle value from enriched DMM of *Workman and Hart* [2005].
[b] DSDP 495 sediments from *Plank and Langmuir* [1998]; B content and δ^{11}B from *Leeman et al.* [2004].
[c] Altered oceanic crust values from *Staudigel et al.* [1996]; B content and δ^{11}B from *Leeman et al.* [2004].
[d] Serpentinite values from *Savov et al.* [2005]; B content and δ^{11}B from *Benton et al.* [2001].
[e] Composition of AOC + Sed fluid assumes a 80:20 mixture AOC-sediment-derived fluids, at 90°C and 30 km (a); 260°C and 70 km (b); and 650°C and 120 km (c). Depth-temperature paths from *Rüpke et al.* [2004] are calculated for a young slab (40 Ma) with subduction rate of 10 cm/yr). To model the B isotope fractionation during dehydration, we used the temperature-dependent B fractionation factor according to *Hervig et al.* [2002] and a partition coefficient of B between hydrous fluids and restitic slab of 0.1 [*Brenan et al.*, 1998]. Model δ^{11}B value and B concentration in restitic material and in released fluids were calculated using the equation by *Marschall et al.* [2006]. Six subsequent stage of dehydration were considered (at 30, 50, 70, 90, 110, and 120 km depth), according to slab dehydration modeled by *Rüpke et al.* [2004]. Water content was assumed to be 7.29% in sediments (GLOSS [*Plank and Langmuir*, 1998]) and 2.7% in the altered igneous oceanic crust, plus 6% of adsorbed, interstitial, and pore water [*Staudigel et al.*, 1996]. Notice that all the adsorbed, interstitial, and pore water and crystalline water from low-grade minerals was lost within the first two steps, with a release of a large amount of B and, particularly, ^{11}B. AOC + Sed (a) and (b) describe fluid evolution with progressive dehydration; only AOC + Sed (c) was used in the model.
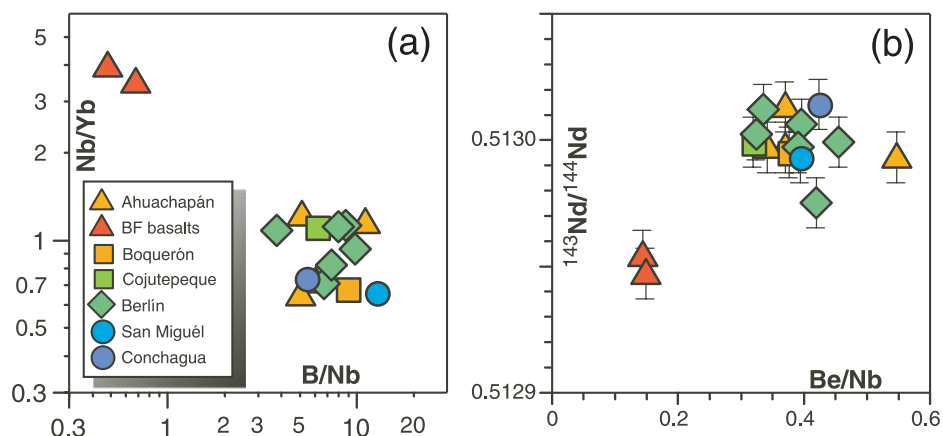
Figure 9. (a) Plot of B/Nb versus Nb/Yb for El Salvador samples. (b) Plot of $^{143}Nd/^{144}Nd$ versus Be/Nb ratios.

from a mantle source metasomatized by a fluid made up of different proportions of (1) a high-^{11}B, water-rich component from a serpentinized, down-dragged mantle in the wedge and/or in the sub-ducted oceanic lithosphere and (2) a low-^{11}B, water-poor component, from subducted altered basaltic crust and oceanic sediments. The occurrence of two distinct fluid components, one ^{11}B-poor and the other ^{11}B-rich, was also suggested by *Morris and Ryan* [2003] to explain the general $\delta^{11}B$ variability in arc magmas.

[29] Within this framework, the boron isotopic signature of the two BF basalts could be explained

by the presence of a smaller amount of fluids, with a strongly reduced serpentinite component (Figure 8). Moreover, the BF basalts have distinctly higher Nb/Yb and lower B/Nb (Figure 9a) and Th/Ta with respect to the volcanic front lavas, indicating that the smaller amount of subduction component is coupled with a lower degree of melting. Their different Nd isotope ratios may be explained in terms of mantle wedge heterogeneity prior to the input from subduction, or ascribed to a subduction component carrying Nd with a $^{143}Nd/^{144}Nd$ that is significantly lower than in the pre-subduction mantle, as for example DSDP 495 sediments, characterized by $^{143}Nd/^{144}Nd$ ratios lower than 0.5127, and
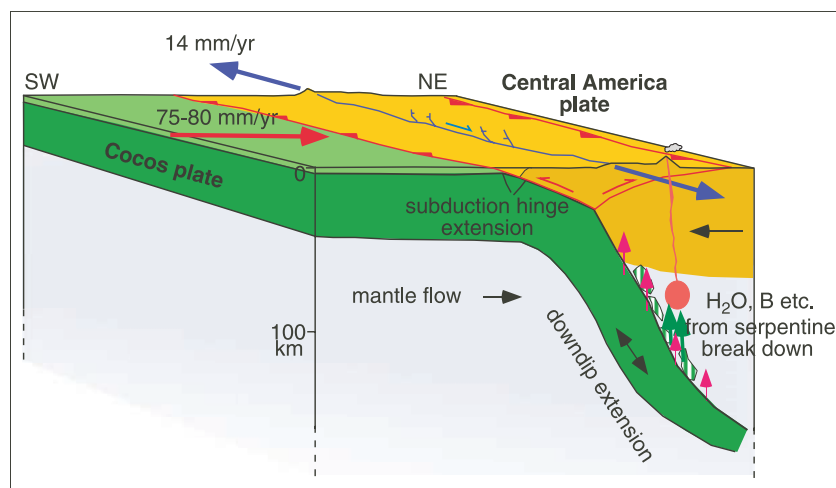

Figure 10. Sketch illustrating the subduction system beneath the El Salvador segment of the Central America Volcanic Arc. Along the Central America subduction zone, the upper plate (Caribbean plate) is undergoing extension due to the far field velocity gradient between the North and South American plates, accommodating an about 14 mm/yr difference. The slab is affected by internal downdip extension, while extension or transtension occurs at the subduction hinge, and thrusting occurs at the plate interface. Right-lateral transtension dominates upper plate deformation. Serpentinized lithosphere may be transported down in subduction, by tectonic erosion. At depths of 100–120 km, serpentine breaks down, releasing water and ^{11}B-rich fluids (green arrows). Pink arrows represent AOC+Sediment-derived fluids.

Table A1. Sample Background

Sample	Rock Type	Place	Geological Setting	Age[a]	Lat., deg N	Long., deg W
ES 50	andesite (lava)	Ahuachapán (Las Chinamas)	volcanic basement[b] (Bálsamo Fmt.)	Miocene-Pleistocene	14.01.16.5	89.54.12.5
ES 43	basalt (lava)	Ahuachapán (Concepción de Ataco)	volcanic basement (Bálsamo Fmt.)	248 ± 67 ka	13.53.08	89.51.20
ES 42	basalt (lava)	Ahuachapán (Cerro de Apaneca)	active volcanic front	Upper Pleist.-Holocene	13.50.27	89.48.35
ES 41	basalt (lava)	Ahuachapán (Juayua)	active volcanic front	Upper Pleist.-Holocene	13.51.25	89.44.20
ES 61	dacite (lava block)	Ahuachapán (Cuyanausul)	active volcanic front	Upper Pleist.-Holocene	13.54.41.2	89.45.42.9
ES 55	basalt (lava)	Ahuachapán (Chalchuapa)	rear-arc monogenetic cones	Upper Pleist.-Holocene	14.02.39.4	89.41.59.1
ES 57	basalt (lava)	Ahuachapán (La Magdalena)	rear-arc monogenetic cones	Upper Pleist.-Holocene	14.03.34.9	89.42.21.1
ES 7	basalt (lava)	Cojutepeque	volcanic basement (Bálsamo Fmt.)	Miocene-Pleistocene	13.43.44	88.55.59
ES 2	basaltic andesite (lava)	Volcán San Salvador (El Boquerón)	active volcanic front	1917 A.D.	13.45.29	89.16.12
ES 45	basalt (dyke)	CA-1 Puente Río Lempa	volcanic basement (Bálsamo Fmt.)	Miocene-Pleistocene	13.37.00	88.33.56
BER 3	basalt (lava)	Berlin	volcanic basement (Bálsamo Fmt.)	Miocene-Pleistocene	13.35.04	88.34.11
ES 46	andesite (lava)	CA-1 Puente Río Lempa	volcanic basement (Bálsamo Fmt.)	415 ± 27 ka	13.39.25	88.42.37
ES 28	basaltic andesite (lava)	Berlin	active volcanic front	Upper Pleist.-Holocene	13.30.07	88.31.13
ES 8	andesite (scoria)	Berlin	active volcanic front	<115 ka	13.31.39	88.29.44
ES 10	dacite (glassy fragment)	Berlin	active volcanic front	Upper Pleist.-Holocene	13.31.39	88.29.44
ES 47	basalt (lava)	Volcán San Miguel	active volcanic front	Upper Pleist.-Holocene	13.30.36	88.14.50
ES 48	basalt (lava)	Volcán Conchagua	active volcanic front	Upper Pleist.-Holocene	13.17.58	87.48.54

[a] Age data from *Agostini et al.* [2006].
[b] Volcanic basement is made up of volcanoclastics, volcanic breccias, and minor lava flows, comprehensively named Balsamo Formation (Miocene-Pleistocene). The Bálsamo Fmt. rocks underlie the products of active volcanoes [see *Agostini et al.*, 2006, and references therein].

Nd contents around 10–20 ppm [*Plank and Langmuir*, 1998; *Patino et al.*, 2000]. This sedimentary component may be added as fluid or melt [*Heydolph et al.*, 2006], but the occurrence of sediment melts should produce higher Be/Nb and Th/Nb than those observed in the BF lavas (Be/Nb ≈ 0.13; Th/Nb ≈ 0.15, Figure 9b).

[30] On the basis of our geochemical data, the occurrence of mantle heterogeneity cannot be excluded, though the lack of any Nd isotope variation along the roughly 300 km of the El Salvador segment of the arc suggests that the pre-subduction mantle had a homogeneous $^{143}Nd/^{144}Nd$ signature. On the whole, the different geochemical features of the two BF basalts may be explained by varying degrees of partial melting of the mantle source modified by different fluid inputs.

6.3. Location of the Serpentinite Reservoir

[31] The collected data has been interpreted via a model in which a serpentinitic, ^{11}B-rich fluid dominates under the volcanic front, though its influence is drastically reduced toward the back-arc region. The occurrence of a serpentinite reservoir in subduction systems has recently been invoked to explain a number of geological, geophysical and geochemical findings [e.g., *Hyndman and Peacock*, 2003; *Hattori and Guillot*, 2003; *Straub and Layne*, 2002; *Stern et al.*, 2006; *Tonarini et al.*, 2006]. However, the location of this reservoir is still a matter of debate, as it could reside either in the subducted oceanic lithosphere or in the mantle wedge. The former has been proposed by *Eiler et al.* [2005] to explain the low oxygen isotope values observed in the CAVA, and by *Rüpke et al.* [2002] and *Ranero et al.* [2003], who suggest that bending-related faulting of the incoming plate promotes serpentinization of the subducting lithosphere. Calculations by *Peacock et al.* [2005], however, indicate that the serpentinized oceanic lithospheric mantle under Nicaragua and Costa Rica at sub-arc depths (115–135 km, 3.5–4.0 GPa) has temperatures lower than 550°C, probably around 450–500°C, well below the serpentine breakdown temperature (≈650°C [*Ulmer and Trommsdorff*, 1995]).

[32] *Hattori and Guillot* [2003] and *Hyndman and Peacock* [2003] have made the general claim that the forearc mantle that has been serpentinized by fluid released in the early subduction stage, can be dragged down by subduction dynamics to the deeper part of the mantle wedge where the bound water is released by serpentine breakdown. Such mantle wedge serpentinites would have higher T values than those predicted at the slab interface (>650°C).

[33] At erosive margins, ^{11}B-rich forearc serpentinites could be dragged to depths of about 100–120 km beneath the volcanic arc by the subducting slab. Mixed fluids from the subducting sediments and AOC and down-dragged serpentinites could trigger partial melting upon migration into the overlying mantle wedge (Figure 10). While AOC and sediment-hosted fluids are released progressively as depth increases [*Rüpke et al.*, 2004], the serpentine-hosted fluids are retained until P-T conditions of serpentine breakdown are reached, when most of the water is released. In such a scenario, serpentinites constitute the main ^{11}B reservoir for metasomatization of the peridotitic mantle-wedge source of volcanic front magmatism.

Appendix A

[34] A detailed description of the samples, including their sampling location, age and geological setting, is reported in Table A1.

Acknowledgment

References

Abers, G. A., T. Plank, and B. R. Hacker (2003), The wet Nicaraguan slab, *Geophys. Res. Lett.*, *30*(2), 1098, doi:10.1029/2002GL015649.

Agostini, S., G. Corti, C. Doglioni, E. Carminati, F. Innocenti, S. Tonarini, P. Manetti, G. Di Vincenzo, and D. Montanari (2006), Tectonic and magmatic evolution of the active volcanic front in El Salvador: Insight into the Berlín and Ahuachapán geothermal areas, *Geothermics*, *35*, 368–408.

Aubouin, J., J. Bourgois, J. Azema, and R. von Huene (1985), Guatemala margin: A model of convergent extensional margin?, *Initial Rep. Deep Sea Drill. Proj.*, *84*, 911–917.

Bebout, G. E., and E. Nakamura (2003), Record in metamorphic tourmalines of subduction-zone devolatilization and boron cycling, *Geology*, *31*, 407–410.

Benton, L. D., J. G. Ryan, and F. Tera (2001), Boron isotope systematics of slab fluids as inferred from a serpentine seamount, Mariana forearc, *Earth Planet. Sci. Lett.*, *187*, 273–282.

Bonatti, E., J. R. Lawrence, and N. Morandi (1984), Serpentinization of oceanic peridotites: Temperature dependence of mineralogy and boron content, *Earth Planet. Sci. Lett.*, *70*, 88–94.

Brenan, J. M., E. Neroda, C. C. Lundstrom, H. F. Show, F. J. Reyerson, and D. L. Phinney (1998), Behaviour of boron, beryllium, and lithium during melting and crystallization: Constraints from mineral-melts partitioning experiments, *Geochim. Cosmochim. Acta*, *62*, 2129–2141.

Carr, M. J. (1984), Symmetrical and segmented variation of physical and geochemical characteristics of the Central American volcanic front, *J. Volcanol. Geotherm. Res.*, *20*, 231–252.

Carr, M. J., and R. E. Stoiber (1990), Volcanism, in *The Geology of North America*, Vol. H, *The Caribbean Region*, edited by G. Dengo and J. E. Case, pp. 375–391, Geol. Soc. of Am., Boulder, Colo.

Carr, M. J., M. D. Fiegenson, and E. A. Bennet (1990), Incompatible element and isotopic evidence for tectonic control of source mixing and melt extraction along the Central American arc, *Contrib. Mineral. Petrol.*, *105*, 369–380.

Carr, M. J., M. D. Fiegenson, L. C. Patino, and J. A. Walker (2004), Volcanism and geochemistry in Central America: Progress and problems, in *Inside the Subduction Factory*, *Geophys. Monogr. Ser.*, vol. 138, edited by J. M. Eiler, pp. 153–174, AGU, Washington, D. C.

Catanzaro, E. J., C. E. Champion, E. L. Garner, G. Malinenko, K. M. Sappenfeld, and W. R. Shields (1970), Boric acid, isotopic, and assay standard reference materials, *U.S. Natl. Bur. Stand. Spec. Publ.*, *260*, 17–70.

Chan, L. H., W. P. Leeman, and C. F. You (2002), Lithium isotopic composition of Central American Volcanic Arc lavas: Implications for modification of subarc mantle by slab-derived fluids, correction, *Chem. Geol.*, *182*, 293–300.

Corti, G., E. Carminati, F. Mazzarini, and M. O. García (2005), Active strike-slip faulting in El Salvador (Central America), *Geology*, *33*, 989–992.

Cruciani, C., E. Carminati, and C. Doglioni (2005), Slab dip vs. lithosphere age: No direct function, *Earth Planet. Sci. Lett.*, *238*, 298–310.

D'Amore, F., and J. T. Mejia (1999), Chemical and physical reservoir parameters at initial conditions in Berlín geothermal field, El Salvador: A first assessment, *Geothermics*, *28*, 45–73.

DeMets, C. (2001), A new estimate for present-day Cocos-Caribbean Plate motion: Implications for slip along the Central American volcanic arc, *Geophys. Res. Lett.*, *28*, 4043–4046.

Dewey, J. W., R. White, and D. A. Hernández (2004), Seismicity and tectonics in El Salvador, in *Natural Hazards in El Salvador*, edited by W. I. Rose et al., *Spec. Pap. Geol. Soc. Am.*, *375*, 363–378.

Dia, A., G. Gruau, G. Olivié-Lauquet, C. Riou, J. Molénat, and P. Curmi (2000), The distribution of rare earth elements in groundwaters: Assessing the role of source-rock composition, redox changes and colloidal particles, *Geochim. Cosmochim. Acta*, *64*, 4131–4151.

D'Orazio, M. (1995), Trace element determination in igneous rocks by ICP-MS: Results on ten international reference samples, *Period. Mineral.*, *64*, 315–328.

Eiler, J. M., M. J. Carr, M. Reagan, and E. Stolper (2005), Oxygen isotope constraints on the sources of Central American arc lavas, *Geochem. Geophys. Geosyst.*, *6*, Q07007, doi:10.1029/2004GC000804.

Feigenson, M. D., and M. J. Carr (1986), Positively correlated Nd and Sr isotope ratio of lavas from Central American volcanic front, *Geology*, *14*, 79–82.

Feigenson, M. D., M. J. Carr, S. V. Maharaj, S. Juliano, and L. L. Bolge (2004), Lead isotope composition of Central American volcanoes: Influence of the Galapagos plume, *Geochem. Geophys. Geosyst.*, *5*, Q06001, doi:10.1029/2003GC000621.

Gonzales Partida, E., V. Torres Rodriguez, and P. Birkle (1997), Plio-Pleistocene volcanic history of the Ahuachapán geothermal system, El Salvador: The Concepciòn de Ataco caldera, *Geothermics*, *26*, 589–612.

Goss, A. R., and S. M. Kay (2006), Steep REE patterns and enriched Pb isotopes in southern Central American arc magmas: Evidence for forearc subduction erosion?, *Geochem. Geophys. Geosyst.*, *7*, Q05016, doi:10.1029/2005GC001163.

Gripp, A. E., and R. G. Gordon (2002), Young tracks of hotspots and current plate velocities, *Geophys. J. Int.*, *150*, 321–361.

Hattori, K., and S. Guillot (2003), Volcanic fronts form as a consequence of serpentinite dehydration in the forearc mantle wedge, *Geology*, *31*(6), 525–528.

Hervig, R. L., G. M. Moore, L. B. Williams, S. M. Peacock, J. R. Holloway, and K. Roggensack (2002), Isotopic and elemental partitioning of boron between hydrous fluid and silicate melt, *Am. Mineral.*, *87*, 769–774.

Heydolph, K., K. Hoernle, P. van den Bogaarb, F. Hauff, and S. Sadofsky (2006), Enriched isotopic composition of the NW Central American Volcanic Arc: Crustal contamination of sediment slab melt? (abstract), *Geochim. Cosmochim. Acta*, *70*, 249.

Husen, S., R. Quintero, E. Kissling, and B. Hacker (2003), Subduction-zone structure and magmatic processes beneath Costa Rica constrained by local earthquake tomography and petrological modelling, *Geophys. J. Int.*, *155*, 11–32.

Hyndman, R. D., and S. M. Peacock (2003), Serpentinization of the forearc mantle, *Earth Planet. Sci. Lett.*, *212*, 417–432.

Ishikawa, T., and E. Nakamura (1994), Origin of the slab component in arc lavas from across-arc variation of B and Pb isotopes, *Nature*, *370*, 205–208.

Ishikawa, T., and F. Tera (1997), Source, composition and distribution of the fluid in Kurile mantle wedge: Constraints from across-arc variations of B/Nb and B isotopes, *Earth. Planet. Sci. Lett.*, *152*, 123–138.

Ishikawa, T., and F. Tera (1999), Two isotopically distinct fluid components involved in the Mariana arc: Evidence from Nb/B ratios and B, Sr, Nd. and Pb isotope systematics, *Geology*, *27*, 83–86.

Ishikawa, T., F. Tera, and E. Nakamura (2001), Boron isotope and trace element systematics of the three volcanic zones in the Kamchatka arc, *Geochim. Cosmochim. Acta*, *65*, 4523–4537.

Le Maitre, R. W. (2002), *Igneous Rocks—A Classification and Glossary of Terms*, 236 pp., Cambridge Univ. Press, Cambridge, U. K.

Leeman, W. P., and V. B. Sisson (1996), Geochemistry of boron and its implications for crustal and mantle processes, in *Boron Mineralogy, Petrology and Geochemistry*, *Rev. Mineral.*, vol. 33, edited by E. S. Grew and L. M. Anovitz, pp. 645–707, Mineral. Soc. of Am., Washington, D. C.

Leeman, W. P., M. J. Carr, and J. D. Morris (1994), Boron geochemistry of the Central America Volcanic Arc: Constraints on the genesis of subduction-related magmas, *Geochim. Cosmochim. Acta*, *57*, 149–168.

Leeman, W. P., S. Tonarini, L. H. Chan, and L. E. Borg (2004), Boron and lithium isotopic variations in a hot subduction zone—The southern Washington Cascades, *Chem. Geol.*, *212*, 101–124.

Marschall, H. R., T. Ludwig, R. Altherr, A. Kalt, and S. Tonarini (2006), Syros metasomatic tourmaline: Evidence for very high-$\delta 11$B fluids in subduction zones, *J. Petrol.*, *47*, 1915–1942.

Martínez-Díaz, J. J., J. A. Álvarez-Gómez, B. Benito, and D. Hernández (2004), Triggering of destructive earthquakes in El Salvador, *Geology*, *32*, 65–68.

McDonough, W. F., and S. S. Sun (1995), The composition of the Earth, *Chem. Geol.*, *120*, 223–253.

Meschede, M. (2003), The Costa Rica convergent margin: A textbook example for the process of subduction erosion, *Neues Jahrb. Geol. Palaeontol. Abh.*, *230*(2–3), 409–428.

Moran, A. E., V. B. Sisson, and W. P. Leeman (1992), Boron in subducted oceanic crust and sediments: Effects of metamorphism and implications for arc magma compositions, *Earth Planet. Sci. Lett.*, *111*, 331–350.

Morris, J. D., and J. G. Ryan (2003), Subduction zone processes and implications for changing composition of the upper and lower mantle, in *Treatise on Geochemistry*, vol. 2, *The Mantle and Core*, edited by H. D. Holland and K. K. Turekian, pp. 451–470, Elsevier, Oxford, U. K.

Morris, J. D., W. P. Leeman, and F. Tera (1990), The subducted component in island arc lavas: Constraints from Be isotopes and B-Be systematics, *Nature*, *344*, 31–36.

Noll, P. D., H. E. Newsom, W. P. Leeman, and J. G. Ryan (1996), The role of hydrothermal fluids in the production of subduction zone magmas: Evidence from siderophile and calcophile trace elements and boron, *Geochim. Cosmochim. Acta*, *60*, 587–612.

Palmer, M. R. (1991), Boron-isotope systematics of Halmahera arc (Indonesia) lavas: Evidence for involvement of the subducted slab, *Geology*, *19*, 215–217.

Patino, L. C., M. J. Carr, and M. D. Feigenson (2000), Local and regional variations in Central American arc lavas controlled by variations in subducted sediment input, *Contrib. Mineral. Petrol.*, *138*, 265–283.

Patino, L. C., M. A. Velbel, J. R. Price, and J. A. Wade (2003), Trace element mobility during spheroidal weathering of basalts and andesites in Hawaii and Guatemala, *Chem. Geol.*, *202*, 343–364.

Peacock, S. M., and R. L. Hervig (1999), Boron isotopic composition of subduction-zone metamorphic rocks, *Chem. Geol.*, *160*, 281–290.

Peacock, S. M., P. E. van Keken, S. D. Holloway, B. R. Hacker, G. A. Abers, and R. L. Fergason (2005), Thermal structure of the Costa Rica—Nicaragua subduction zone, *Phys. Earth Planet. Inter.*, *149*, 187–200.

Plank, T., and C. H. Langmuir (1998), The geochemical composition of subducting sediment and its consequences for the crust and mantle, *Chem. Geol.*, *145*, 325–394.

Protti, M., F. Guendel, and K. McNally (1995), Correlation between age of the subducting Cocos Plate and geometry of the Wadati-Benioff zone under Nicaragua and Costa Rica, *Spec. Pap. Geol. Soc. Am.*, *295*, 309–326.

Ranero, C. R., and R. von Huene (2000), Subduction erosion along the Middle America convergent margin, *Nature*, *404*, 748–752.

Ranero, C. R., J. P. Phipps Morgan, K. McIntosh, and C. Reichert (2003), Bending-related faulting and mantle serpentinization at Middle America trench, *Nature*, *425*, 367–373.

Reagan, M. K., J. D. Morris, E. A. Herrstrom, and M. T. Murrell (1994), Uranium series and beryllium isotope evidence for an extended history of subduction modification of the mantle below Nicaragua, *Geochim. Cosmochim. Acta*, *58*, 4199–4212.

Rose, E. F., N. Shimizu, G. D. Layne, and T. L. Grove (2001), Melt production beneath Mt. Shasta from boron data in primitive melt inclusions, *Science*, *293*, 281–283.

Rüpke, L. H., J. Phipps Morgan, M. Hort, and J. A. D. Connolly (2002), Are the regional variations in Central American arc lavas due to differing basaltic versus peridotitic slab sources of fluids?, *Geology*, *30*, 1035–1038.

Rüpke, L. H., J. Phipps Morgan, M. Hort, and J. A. D. Connolly (2004), Serpentine and the subduction zone water cycle, *Earth Planet. Sci. Lett.*, *223*, 17–34.

Savov, I. P., J. G. Ryan, M. D'Antonio, K. Kelley, and P. Mattie (2005), Geochemistry of serpentinized peridotites from the Mariana Forearc Conical Seamount, ODP Leg 125: Implications for the elemental recycling at subduction zones, *Geochem. Geophys. Geosyst.*, *6*, Q04J15, doi:10.1029/2004GC000777.

Smith, H. J., A. J. Spivack, H. Staudigel, and S. R. Hart (1995), The boron isotopic composition of altered oceanic crust, *Chem. Geol.*, *126*, 119–135.

Spivack, A. J., and J. M. Edmond (1987), Boron isotope exchange between seawater and the oceanic crust, *Geochim. Cosmochim. Acta*, *51*, 1033–1043.

Staudigel, H., T. Plank, W. M. White, and H. Schmincke (1996), Geochemical fluxes during seafloor alteration of the upper oceanic crust: DSDP Sites 417 and 418, in *Subduction Top to Bottom*, *Geophys. Monogr. Ser.*, vol. 96, edited by G. E. Bebout et al., pp. 19–38, AGU, Washington, D. C.

Stern, R. J., E. Kohut, S. H. Bloomer, M. Leybourne, M. Fouch, and J. Vervoort (2006), Subduction factory processes beneath the Guguan cross-chain, Mariana Arc: No role for sediments, are serpentinites important?, *Contrib. Mineral. Petrol.*, *151*, 202–221.

Straub, S. M., and G. D. Layne (2002), The systematics of boron isotopes in Izu arc front volcanic rocks, *Earth Planet. Sci. Lett.*, *198*, 25–39.

Syracuse, E. M., and G. A. Abers (2006), Global compilation of variations in slab depth beneath arc volcanoes and implications, *Geochem. Geophys. Geosyst.*, *7*, Q05017, doi:10.1029/2005GC001045.

Tanaka, T., et al. (2000), JNdi-1: A neodymium isotopic reference in consistency with LaJolla neodymium, *Chem. Geol.*, *168*, 279–281.

Tatsumi, Y., and S. Eggins (1995), *Subduction Zone Magmatism*, 221 pp., Blackwell Sci., Cambridge, Mass.

Taylor, S. R., and S. M. McLennan (1995), The geochemical evolution of the continental crust, *Rev. Geophys.*, *33*(2), 241–265.

Todt, W., R. A. Cliff, A. Hanser, and A. W. Hofmann (1993), Re-calibration of NBS lead standards using a ^{202}Pb-^{205}Pb double spike, *Terra Abstr.*, *5*(1), 396.

Tonarini, S., M. Pennisi, A. Adorni-Braccesi, A. Dini, G. Ferrara, R. Gonfiantini, M. Wiedenbeck, and M. Gröning (2003), Intercomparison of boron isotope and concentration measurements: Part I: Selection, preparation and homogeneity tests of the intercomparison materials, *Geostand. Newsl.*, *27*, 21–39.

Tonarini, S., S. Agostini, F. Innocenti, and P. Manetti (2005), δ^{11}B as tracer of slab dehydration and mantle evolution in western Anatolia Cenozoic magmatism, *Terra Nova*, *17*, 259–264.

Tonarini, S., W. P. Leeman, F. Innocenti, M. D'Orazio, and P. T. Leat (2006), The boron transfer from the slab to the mantle wedge: A combined study in South Sandwich Island Arc and Southern Volcanic Zone in the Chile Andes, *Eos Trans. AGU*, *87*(36), Jt. Assem. Suppl., Abstract V33A-06.

Ulmer, P., and V. Trommsdorff (1995), Serpentine stability to mantle depths and subduction-related magmatism, *Science*, *268*, 858–861.

Vannucchi, P., S. Galeotti, P. D. Clift, and R. von Huene (2004), Long-term subduction-erosion along the Guatemalan margin of the Middle America Trench, *Geology*, *32*, 617–620.

Walker, J. A., M. J. Carr, L. C. Patino, C. M. Johnson, M. D. Feigenson, and R. L. Ward (1995), Abrupt change in magma generation processes across the Central American arc in southeastern Guatemala: Flux-dominated melting near the base of the wedge to decompression melting near the top of the wedge, *Contrib. Mineral. Petrol.*, *120*, 378–390.

Walker, J. A., L. C. Patino, B. I. Cameron, and M. J. Carr (2000), Petrogenetic insights provided by compositional transects across the Central American arc: Southeastern Guatemala and Honduras, *J. Geophys. Res.*, *105*, 18,949–18,963.

Workman, R. K., and S. R. Hart (2005), Major and trace element composition of the depleted MORB mantle (DMM), *Earth Planet. Sci. Lett.*, *231*, 53–72.

You, C. F., A. J. Spivack, J. M. Gieskes, R. Rosenbauer, and J. L. Bischoff (1995), Experimental study of boron geochemistry: Implications for fluid processes in subduction zones, *Geochim. Cosmochim. Acta*, *59*, 2435–2442.